Published in final edited form as:
Biochemistry. 2013 September 24; 52(38): 6702–6711. doi:10.1021/bi401041v.

Discrimination of RNA *versus* DNA by polynucleotide phosphorylase

Mihaela-Carmen Unciuleac and **Stewart Shuman***
Molecular Biology Program, Sloan-Kettering Institute, New York, NY 10065 USA

Abstract

Polynucleotide phosphorylase (PNPase) plays synthetic and degradative roles in bacterial RNA metabolism; it is also suggested to participate in bacterial DNA transactions. Here we used chimeric polynucleotides, composed of alternating RNA and DNA tracts, to analyze whether and how *Mycobacterium smegmatis* PNPase discriminates RNA *versus* DNA during the 3' phosphorolysis reaction. We find that a kinetic block to 3' phosphorolysis of a DNA tract within an RNA polynucleotide is exerted when resection has progressed to the point that a 3' monoribonucleotide flanks the impeding DNA segment. The position of the pause one nucleotide upstream of the first deoxynucleotide encountered is independent of DNA tract length. However, the duration of the pause is affected by DNA tract length, being transient for a single deoxynucleotide and durable when two or more consecutive deoxynucleotides are encountered. Substituting manganese for magnesium as the metal cofactor enables PNPase to "nibble" into the DNA tract. A 3'-phosphate group prevents RNA phosphorolysis when the metal cofactor is magnesium. With manganese, PNPase can resect an RNA 3'-phosphate end, albeit 80-fold slower than a 3'-OH. We discuss the findings in light of the available structures of PNPase and of the archaeal exosome•RNA•phosphate complex and propose a model for catalysis whereby the metal cofactor interacts with the scissile phosphodiester and the penultimate ribose.

Polynucleotide phosphorylase[1] (PNPase) catalyzes step-wise phosphorolysis of the 3'-terminal phosphodiesters of RNA chains to yield nucleoside diphosphate (NDP) products. In the reverse reaction PNPase acts as a polymerase, using NDPs as substrates to add NMPs to the 3'-OH terminus of RNA chains while expelling inorganic phosphate (P_i). The RNA phosphorylase and polymerase activities require a divalent cation, which can be either magnesium or manganese. PNPase also acts on DNA polynucleotides as a DNA 3'-phosphorylase and a dADP-dependent DNA polymerase. The DNA modification reactions of PNPase depend on manganese and are not sustained effectively by magnesium.

Whereas the relevance of PNPase to bacterial RNA decay and post-transcriptional 3'-tailing is supported by genetic studies[2] in model organisms, its role in DNA transactions is an open question. Based on analysis of the effects of a *Bacillus subtilis ΔpnpA* null allele on clastogen sensitivity and its epistasis relationships to null alleles of DNA repair factors, Alonso and colleagues concluded that PNPase participates in the homologous recombination (HR) and nonhomologous end joining (NHEJ) pathways of *B. subtilis* double-strand break (DSB) repair.[3] They suggest that PNPase reacts with broken DNA ends, either converting them from non-ligatable "dirty" breaks to clean ends that can be sealed by DNA ligase or by adding non-templated single-stranded 3' tails that can then influence repair pathway choice.[3,4]

*correspondence: 212-639-7145; s-shuman@ski.mskcc.org.

Our interest in the multiple pathways of DSB repair in mycobacteria[5–9] prompted us to characterize and compare the RNA and DNA modifying activities of PNPase from *Mycobacterium smegmatis*.[10] Like other PNPases, the *M. smegmatis* protein is a homotrimer of a polypeptide composed of five domain modules (Fig. 1A). Crystal structures of exemplary PNPases have shown that the enzyme is ring-shaped, with a central channel within which the active site is located.[11–15] Two RNase PH-like domains form the core of the trimeric ring (Fig. 1B). The metal-binding site is located within the distal PH domain (Fig. 1A).[13] An α-helical module separating the PH domains is disposed on the inferior surface of the ring. The C-terminal KH and S1 domains are on the opposite face of the ring and are conformationally mobile (Fig. 1B). The three KH modules of the *Caulobacter* PNPase trimer form a narrow aperture that contacts the RNA and through which a single-stranded polynucleotide is threaded *en route* to the central cavity.[15]

As expected, *M. smegmatis* PNPase is a Mg^{2+}•PO_4-dependent RNA 3'-phosphorylase and Mg^{2+}•ADP-dependent RNA polymerase.[10] The enzyme is also a Mn^{2+}•dADP-dependent DNA polymerase and a Mn^{2+}•PO_4-dependent DNA 3'-phosphorylase.[10] The unexpected finding was that deletions of the C-terminal S1 and KH domains of mycobacterial PNPase exerted opposite effects on the RNA and DNA modifying activities.[10] Deleting the S1 domain reducd RNA phosphorylase and polymerase activity; deletion of the S1 and KH domains further compromised the enzyme with respect to RNA substrates. By contrast, the S1 and KH deletions increased the DNA polymerase and phosphorylase activity. We observed two distinct modes of nucleic acid binding by mycobacterial PNPase: (i) metal-independent RNA-specific binding via the S1 domain, and (ii) metal-dependent binding to RNA or DNA that is optimal when the S1 domain is deleted.[10] These findings enhanced our understanding of PNPase specificity, whereby the C-terminal modules serve two roles: (i) to help engage an RNA polynucleotide substrate for processive 3' end additions or resections, and (ii) to act as a specificity filter that disfavors a DNA polynucleotide substrate.

Here, we delve deeper into the means by which *M. smegmatis* PNPase discriminates RNA from DNA by studying the phosphorolysis of chimeric polynucleotides, composed of alternating RNA and DNA tracts. We also interrogate the ability of PNPase to resect a "dirty" end with a non-ligatable 3'-PO_4.

EXPERIMENTAL PROCEDURES

M. smegmatis PNPase

The 763-aa wild-type PNPase polypeptide and a truncated variant PNPase-(1–656) lacking the S1 domain (ΔS1), were produced in *E. coli* as His_{10}-tagged derivatives, as were mutated versions in which the putative metal-binding Asp526 and Asp532 residues were changed to alanine. The recombinant PNPase proteins were purified from soluble bacterial extracts by sequential nickel-affinity, anion-exchange, and gel-filtration chromatography steps as described previously.[10] Protein concentrations were determined by using the Bio-Rad dye reagent with BSA as the standard.

3'-phosphorylase assay

Synthetic 24-mer oligonucleotides were 5' ^{32}P-labeled by using T4 polynucleotide kinase and [γ-^{32}P]ATP and then purified by electrophoresis through a native 18% polyacrylamide gel. Phosphorylase reaction mixtures (10 μl) containing 20 mM Tris-HCl (pH 7.5), 0.1 μM of 5' ^{32}P-labeled 24-mer substrate, $MgCl_2$ or $MnCl_2$, $(NH_4)_2PO_4$, and PNPase as specified (expressed as pmol or concentration of PNPase protomer) were incubated at 37°C. The reactions were quenched by adding 10 μl of 90% formamide, 50 mM EDTA. The samples were heated for 5 min at 100°C and then analyzed by electrophoresis through a 40-cm 20%

polyacrylamide gel containing 7.5 M urea in 44.5 mM Tris-borate (pH 8.3), 1 mM EDTA. The radiolabeled RNAs were visualized by autoradiography and, where specified, quantified by scanning the gel with a Fujifilm BAS-2500 imager.

Resection of 3' end-labeled polynucleotides with 3'-OH versus 3'-PO_4 termini

A 25-mer RNA substrate with a 3'-PO_4 terminus and a ^{32}P-label at the 3' phosphodiester was prepared by T4 RNA ligase-mediated addition of [5'-^{32}P]pCp to a 24-mer RNA as described[16] and then gel-purified. The radiolabeled RNAp strand was treated with calf intestine alkaline phosphatase to generate a 3'-OH derivative, RNA_{OH}, which was gel-purified. Phosphorolysis reaction mixtures (70 μl) containing 20 mM Tris-HCl (pH 7.5), either 5 mM $MgCl_2$ and 0.5 mM $(NH_4)_2PO_4$ or 5 mM $MnCl_2$ and 30 μM $(NH_4)_2PO_4$, 0.1 μM 3' ^{32}P-labeled 25-mer RNAp or RNA_{OH} substrates, and 0.3 μM PNPase protomer were incubated at 37°C. Aliquots (10 μl) were withdrawn at the times specified and quenched by adding 1 μl of 0.5 M EDTA. Aliquots (2 μl) of each sample were analyzed by PEI cellulose TLC with 0.45 M ammonium sulfate as the mobile phase. Cold CDP was analyzed in parallel and visualized by UV illumination of the TLC plate. The radiolabeled species were visualized by autoradiography. The remaining 9 μl of each sample was analyzed by urea-PAGE.

Gel-shift assay of nucleic acid binding

Reaction mixtures (10 μl) containing 20 mM Tris-HCl (pH 7.5), 10% glycerol, 0.1 μM (1 pmol) of 5' ^{32}P-labeled 24-mer single-strand RNA (shown in Fig. 1D), 40 pmol of wild-type or mutant PNPase protomer as specified, and either no metal or 5 mM $MnCl_2$ were incubated for 20 min on ice. The mixtures were adjusted to 20% glycerol and then analyzed by electrophoresis through a 15-cm native 6% polyacrylamide gel containing 22.5 mM Tris borate, 0.625 mM EDTA. The gel was run at 110 V in the cold room for 3 h and then dried under vacuum on DE81 paper. The free ^{32}P-labeled RNA and slower migrating PNPase•[^{32}P]-nucleic acid complexes were visualized by autoradiography of the dried gel.

RESULTS

Metal-dependent RNA binding by the PNPase core trimer

Incubation of recombinant full-length (FL) PNPase with a 5' ^{32}P-labeled 24-mer RNA in the absence of metal, phosphate, or ADP (to preclude the phosphorylase and polymerase activity) resulted in the formation of a discrete PNPase•RNA complex that was well resolved from free RNA during native PAGE (Fig. 1D). By contrast, the ΔS1 protein did not bind to the 24-mer RNA in the absence of divalent cation (Fig. 1D). However, when the RNA binding reactions were performed in the presence of 5 mM manganese, the full-length and ΔS1 PNPases both formed stable PNPase•RNA complexes (Fig. 1D). The same holds when the binding reactions are performed in the presence of magnesium.[10]

To gauge whether the metal-dependent binding of nucleic acid to PNPase is mediated by divalent cation(s) in the active site, we mutated the predicted binding site for the metal cofactor. The crystal structure of *E. coli* PNPase in complex with Mn^{2+} had identified Asp486 and Asp492 within the peptide ^{486}**D**HLGDM**D**^{492} as direct metal ligands.[13] The equivalent motif in the distal PH domain of *M. smegmatis* PNPase is ^{526}**D**AFGDM**D**^{532} (Fig. 1A and C). Previous studies showed that replacing the distal metal-binding Asp492 residue of *E. coli* PNPase with glycine abolished phosphorylase activity[17], as did the equivalent Asp-to-Gly mutation of *Bacillus* PNPase[4]. We reported that the Mn^{2+}•DNA and Mg^{2+}•RNA end modifying activities of *M. smegmatis* PNPase are coordinately suppressed by mutating the proximal metal-binding Asp526 residue to alanine[10]. Here we find that the D526A mutation of the full-length and ΔS1 PNPases did not affect manganese-dependent

binding to RNA, nor did a D526A–D532A double-mutation of the full-length and ΔS1 PNPases (Fig. 1D). Also, the D526A and D526A–D532A mutations did not affect magnesium-dependent RNA binding to the full-length and ΔS1 PNPases (not shown). We surmise that the metal effect on RNA binding by the mycobacterial PNPase core trimer is likely not dictated by the metal catalyst(s) of phosphoryl transfer in the active site. The results suggest the existence of additional metal interactions with the polynucleotide substrate and/or the PNPase protein that promote stable binding to nucleic acid in the absence of the S1 domain.

DNA imposes a kinetic obstacle to 3' phosphorolysis

To gain insights to the discrimination between DNA and RNA during catalysis of 3' end resection, we presented full-length and ΔS1 PNPase with a series of 5' ^{32}P-labeled 24-mer substrates: composed entirely of ribonucleotides (pRNA$_{OH}$) or deoxyribonucleotides (pDNA$_{OH}$); or comprising chimeras in which the 5' 12 nucleotides were DNA and the 3' 12 nucleotides RNA (pDNA•RNA$_{OH}$) or the 5' 12 nucleotides were RNA and the 3' 12 nucleotides DNA (pRNA•DNA$_{OH}$) (Fig. 2A). We reacted these 24-mers with PNPase in the presence of 30 μM phosphate and either 5 mM magnesium or manganese. (Prior studies[10] showed that 30 μM phosphate was optimal for phosphorylase activity in the presence of manganese.) The products were analyzed by urea-PAGE and the labeled RNAs visualized by autoradiography (Fig. 2A and B). FL and ΔS1 PNPase resected the 3' end of the pRNA$_{OH}$ strand in the presence of either magnesium or manganese to yield a ladder terminating in trinucleotide and mononucleotide products. By contrast, the PNPases failed to shorten the pDNA$_{OH}$ substrate in the presence of magnesium and catalyzed limited phosphorolysis of pDNA$_{OH}$ in the presence of manganese, resecting up to five deoxynucleotides (Fig. 2A and B). The pRNA•DNA$_{OH}$ substrate fared little better than the all-DNA strand, insofar as it was virtually unreactive with PNPase in magnesium, and was weakly reactive in manganese. The size distribution of the products of pRNA•DNA$_{OH}$ phosphorolysis in manganese indicated that a minority of the strands (14%) had undergone resection of the 3' DNA segment and subsequent trimming of the resulting 5' RNA oligonucleotide.

The most instructive findings pertained to the action of FL and ΔS1 PNPase on the pDNA•RNA$_{OH}$ substrate, whereby the 3' RNA segment was resected in the presence of either metal, but the phosphorolysis reaction was arrested at different positions in magnesium *versus* manganese. The product ladder indicated clearly that the major product of the reaction of FL and ΔS1 PNPase with pDNA•RNA$_{OH}$ in magnesium had undergone eleven cycles of phosphorolysis to yield a radiolabeled species – p(dGGGTCGCAATTG)(rA)$_{OH}$ – that migrated 1-nucleotide step above a 5' ^{32}P-labeled p(dGGGTCGCAATTG)$_{OH}$ reference strand (Fig. 2A and B). Thus, the impediment to DNA resection in magnesium is apparently not exerted by the identity of the 3' terminal nucleotide sugar (which is a ribose at the point of reaction arrest in this experiment), but rather by the sugar identity at one or more of the penultimate nucleotides. In the presence of manganese, ΔS1 PNPase proceeded past this point, yielding products corresponding to p(dGGGTCGCAATTG)$_{OH}$, p(dGGGTCGCAATT)$_{OH}$, and p(dGGGTCGCAAT)$_{OH}$ (Fig. 2B).

The time course of pDNA•RNA$_{OH}$ phosphorolysis by ΔS1 PNPase (Fig. 3) verified that the pD12R1$_{OH}$ species is a stable kinetic end-product when magnesium is the cofactor. With manganese, the pD12R1$_{OH}$ species accumulates early (at 1 min) and then converted to pD12$_{OH}$ and pD11$_{OH}$ with longer incubation. The pD12R1$_{OH}$, pD12$_{OH}$ and pD11$_{OH}$ products comprised 22%, 44% and 20% of the total labeled material at 15 min.

A segment of four internal deoxynucleotides suffices to arrest phosphorolysis

To better elucidate the basis for the arrest of phosphorolysis by DNA, we prepared a 5' ^{32}P-labeled 24-mer substrate composed of an 8-nucleotide 5' RNA segment, followed by a 4-nucleotide internal DNA tract, and a 12-nucleotide 3' RNA segment. Mild alkaline hydrolysis of the labeled $pR_8D_4R_{12OH}$ strand confirmed the presence of four alkali-resistant phosphodiester linkages corresponding to the internal DNA tract (Fig. 4, lane OH). We reacted 0.1 μM $pR_8D_4R_{12OH}$, or an all-RNA 24-mer control, with and equimolar level of PNPase (as trimer), 5 mM magnesium, and 0.5 mM phosphate (an optimum phosphate concentration for magnesium-dependent phosphorolysis[10]). PNPase converted the bulk of the all-RNA 24-mer to trinucleotide or mononucleotide products within 10 s (Fig. 4, left), at which time the trinucleotide predominated (trinucleotide/mononucleotide = 3.8). Further incubation resulted in progressive conversion of the labeled trinucleotide to a mononucleotide end-product, e.g., the trinucleotide/mononucleotide value at 5 min was 0.05. By contrast, processing of the $pR_8D_4R_{12OH}$ strand was arrested after 11 steps of 3' nucleotide removal to yield a $pR_8D_4R_{OH}$ product that persisted for at least 5 min (Fig. 4, right). A small fraction of the $pR_8D_4R_{OH}$ strand (11% at 5 min) was slowly processed to pR_8D_{4OH} and then through the intervening DNA to yield trinucleotide and mononucleotide species. These experiments show that four consecutive deoxynucleotides suffice to form a kinetic block to phosphorolysis by mycobacterial PNPase

Effect of internal DNA tract length on phosphorolysis

We extended the analysis of chimeric 24-mer substrates to $pR_9D_3R_{12OH}$, $pR_{10}D_2R_{12OH}$, and $pR_{11}D_1R_{12OH}$ variants that contained internal tri-, di-, and mono-deoxynucleotide tracts within an otherwise all-RNA polynucleotide of identical nucleobase sequence. The kinetic profile of phosphorolysis of the 5' ^{32}P-labeled $pR_9D_3R_{12OH}$ strand (Fig. 5) showed that reaction was arrested after 11 steps of phosphorolysis, with the $pR_9D_3R_{OH}$ product lingering for at least 5 min, at which time only 5% of the $pR_9D_3R_{OH}$ species was resected past the trinucleotide DNA segment to yield smaller end products. Processing of the $pR_{10}D_2R_{12OH}$ substrate was durably halted at the same position; the extent of "read-through" of the internal DNA dinucleotide at 5 min was 17%. By contrast, a single internal deoxynucleotide in the $pR_{11}D_1R_{12OH}$ substrate elicited a transient pause after 11 steps of phosphorolysis; the paused $pR_{11}D_1R_{OH}$ species accumulated at 15 and 30 s, then declined steadily at 1, 2 and 5 min, concomitant with an increase in trinucleotide and mononucleotide end-products. The extent of read-through at 5 min was 96%. These results indicate that: (i) DNA induces a kinetic obstacle to 3' phosphorolysis by PNPase at a position 1 nucleotide upstream of the first deoxynucleotide encountered (upstream with respect to the direction of phosphorolysis); (ii) the position of the pause is independent of DNA tract length; (iii) the duration of the DNA-induced pause is affected by DNA tract length, being transient for a single deoxynucleotide and durable when two or more consecutive deoxynucleotides are encountered.

Can PNPase process a "dirty" 3'-PO_4 end?

Genetic evidence implicating *Bacillus* PNPase in the repair of DNA damage inflicted by hydrogen peroxide led to the suggestion that the enzyme's 3' phosphorylase activity might trim non-ligatable "dirty" single-stranded DNA ends.[3,4] One of the dirty lesions resulting from oxidative damage is a 3'-phosphate. One can envision two possible pathways by which PNPase might process a 3'-phosphate end: (i) phosphorolytic attack on the 3'-phosphomonoester to yield inorganic pyrophosphate and a 3'-OH polynucleotide of the same length; or (ii) phosphorolytic attack on the vicinal –N**p**Np phosphodiester to yield ppNp and a shortened 3'-OH polynucleotide. To probe whether either of these outcomes occurs, we prepared a 25-mer RNAp substrate with a 3'-monophosphate and a single ^{32}P-label at the

terminal –G**p**Cp phosphodiester (Fig. 6). This substrate was reacted with PNPase in the presence of magnesium and 0.5 mM phosphate. The products were analyzed by PEI-cellulose TLC (to track the liberation of a labeled phosphorolysis product) and denaturing PAGE (to monitor the decay of the input 25-mer RNA). As a positive control, we reacted PNPase in parallel with an otherwise identical 25-mer RNA_{OH} substrate with a 3'-OH and a ^{32}P-label at the terminal –G**p**C_{OH} phosphodiester. Whereas the input ^{32}P-labeled 25-mer RNA remained at the origin during TLC, the reaction of PNPase with the RNA_{OH} substrate resulted in release of the radiolabel as ^{32}P-CDP (Fig. 6A, left). We observed concordant disappearance of the input 25-mer when the products were analyzed by denaturing PAGE (Fig. 6B, left). (The released mononucleotide migrated diffusely near the solute front during PAGE; not shown). By contrast, the RNAp substrate was refractory to phosphorolysis by PNPase (Fig. 6A and B, right). A quantification of the time course of ^{32}P-CDP release from the RNA_{OH} and RNAp substrates in the presence of magnesium is shown in Fig. 7A. When the phosphorolysis reactions were performed in the presence of manganese and 30 μM phosphate, we were able to detect ^{32}P-CDP release from the RNAp strand, albeit at a rate that was 80-fold less than the rate of ^{32}P-CDP release from the RNA_{OH} strand (Fig. 7B). We surmise that mycobacterial PNPase does not provide a vigorous 3' end-healing function at a 3'-PO_4 RNA end.

DISCUSSION

Our studies of the polynucleotide substrate specificity of mycobacterial PNPase are aimed at clarifying an emerging picture of PNPase as a catalyst of DNA transactions in addition to its synthetic and degradative functions in RNA metabolism. The new findings here concern three aspects of PNPase function: (i) the distinctions between the metal-independent and metal-dependent modes of nucleic acid binding; (ii) the sensitivity of the 3' phosphorylase reaction to blockage by DNA; and (iii) the capacity of PNPase to resect a polynucleotide with a 3'-phosphate end instead of a 3'-OH.

Experiments using a gel-shift assay to gauge nucleic acid binding to mycobacterial PNPase implicated the S1 domain as an RNA selectivity filter, by virtue of its ability to confer RNA-specific binding in the absence of a divalent cation.[10] When the S1 domain is deleted, the ΔS1 PNPase binds to *either* RNA or DNA in a distinct mode that requires a divalent cation.[10] In suggesting a direct role of the manganese-dependent activities of *Bacillus* PNPase in DNA repair, Cardenas et al.[3] proposed that PNPase interacts with single-stranded DNA through its S1 domain. Yet, our results with the ΔS1 mutant, here and previously, are inimical to that model, especially insofar as the DNA polymerase activity of mycobacterial ΔS1 PNPase is higher than that of the full-length PNPase.[10] Our initial expectation was that the metal requirement for nucleic acid binding in the absence of the S1 domain would reflect capture of the RNA 3'-terminus by manganese ion(s) engaged in the PNPase active site. However, the finding that elimination of the two conserved aspartate residues in the active site that comprise the manganese binding site of *E. coli* PNPase[13] did not affect the formation of a stable PNPase-nucleic acid complex casts doubt on this idea. An alternative explanation is that divalent metals exert their impact by binding to the single-stranded polynucleotide chain, the core PNPase trimeric ring, or both. Analyses of manganese cocrystals of *E. coli* PNPase[13] and of the *Sulfolobus solfataricus* exosome[18] (an archaeal PNPase homolog) have highlighted the capacity for metal-binding at sites remote from the catalytic pocket.

The prior suggestion[4] that the 3' phosphorylase activity of PNPase might serve to clean and remodel non-ligatable dirty ends was put to the test here. Specifically, by comparing PNPase action on otherwise identical single-stranded polynucleotides with 3'-phosphate versus 3'-OH ends, we found that a 3'-phosphate group prevented phosphorolysis when the metal

cofactor was magnesium. When the cofactor was manganese, the rate of resection of the 3'-phosphate end was slower by a factor 80 that the rate of resection of the 3'-OH control substrate. Insights to the basis for this blockade can be gleaned from the co-crystal structure of the *Sulfolobus* exosome with RNA and phosphate engaged in the active site in a putative pre-catalytic state of the phosphorolysis reaction (pdb 4BA2).[19] A stereo view of the *Sulfolobus* complex is shown in Fig. 8, with the inorganic phosphate substrate (PO_4, with phosphorus atom colored yellow) adjacent to the RNA 3'-terminal phosphodiester (labeled P1, with the phosphorus atom colored green). The inorganic phosphate oxygen nucleophile is 3.7 Å from the phosphodiester phosphorus in a nearly perfect apical orientation (174°) to the ribose O3' leaving group of the penultimate RNA nucleotide (which will become the 3'-OH of the resected RNA product). We regard the archaeal exosome as a plausible model for the pre-catalytic state of the PNPase phosphorolysis reaction, in light of the similar folds of the respective domain modules and active sites and the identity/similarity of most of the active site amino acids that contact the phosphate and RNA ligands. (To that end, the conserved amino acids in the archaeal exosome structure depicted in Fig. 8 are labeled and numbered according to their identity and position in *M. smegmatis* PNPase.)

The structure suggests how hydrogen-bonding by the terminal ribose O3' with the inorganic phosphate anion might provide a mechanism of substrate assisted catalysis, which would be lacking if the terminal nucleoside was subtracted, as would be the case for a 3'-phosphate polynucleotide substrate bound to PNPase with the terminal phosphate in the P1 site. In addition, the structure shows how hydrogen bonding of the ribose O3' and O2' atoms to nearby main-chain amide nitrogen and carbonyl oxygen atoms of PNPase tethers the terminal nucleotide and thus helps ensure a proper orientation of the P1 phosphodiester with respect to the inorganic phosphate nucleophile. We envision that subtraction of the 3' nucleoside would increase the conformational freedom of a polynucleotide 3'-monophosphate in the P1 site and thereby contribute to the feeble ability of PNPase to resect such an end. An alternative explanation is that the 3'-phosphate polynucleotide substrate binds to PNPase with the terminal phosphate in the PO_4 site, thereby precluding binding of the inorganic phosphate substrate.

Our findings that mycobacterial PNPase was inept at phosphorolysis at a 3'-phosphate RNA end in the presence of magnesium resonate with classic studies by Singer and colleagues of *Micrococcus luteus* PNPase,[20,21] wherein they found that an isomeric mixture of oligoadenylates with 2'-phosphate and 3'-phosphate ends was resistant to phosphorolysis. Moreover, an isomeric mixture of $(Ap)_5A$ with 2'-phosphate and 3'-phosphate ends inhibited the phosphorolysis of $(Ap)_5A_{OH}$. This inhibition was competitive with respect to the RNA_{OH} substrate but non-competitive with respect to inorganic phosphate, consistent with binding of the RNAp inhibitor in the active site with the terminal 3'-phosphate in the P1 site. Here we found that manganese in lieu of magnesium allowed a feeble rate of RNAp phosphorolysis by mycobacterial PNPase. Because the ^{32}P-labeled product comigrated during TLC with the ^{32}P-CDP formed by phosphorolysis of RNA_{OH} (not shown), we infer that the phosphorolysis of the terminal nucleotide was preceded by the rate-limiting step of removing the 3'-phosphate group (presumably via phosphorolysis to yield PP_i). Although we cannot exclude the possibility that PNPase might contribute to a manganese-dependent metabolism of non-ligatable polynucleotide 3' ends *in vivo*, we think this is an unlikely scenario, given that mycobacteria and other bacterial taxa have a dedicated manganese-dependent DNA 3' end-healing enzyme – the 3'-phosphoesterase (PE) domain of DNA ligase D – built in to their machinery for non-homologous end-joining of DNA double-strand breaks.[22,23]

The surprising finding (to us) of the present study was that the kinetic block to 3' phosphorolysis of a DNA tract within an RNA polynucleotide is exerted when resection has

progressed to the point that a 3' monoribonucleotide flanks the impeding DNA segment. Our (naive) expectation was that the phosphorolysis reaction would remove all of the 3' ribonucleotides and arrest when the first 3' deoxynucleotide occupies the terminal nucleotide position (N1) in the PNPase active site. Instead, our results suggest that the reaction pauses with a 3' ribonucleotide in the N1 position and a deoxynucleotide at N2.

The crystal structure of the homologous archaeal exosome[19] reveals the location and contacts of the terminal tetranucleotide RNA segment (Fig. 8) and offers clues to the basis for the kinetic behavior of mycobacterial PNPase during phosphorolysis of an all-RNA strand *versus* a polynucleotide punctuated by a DNA tract. The N1, N2, N3 and N4 nucleobases (numbered from the 3' end) form a continuous base stack, capped by the enzyme via a π stack of an aromatic side chain (a tyrosine in the archaeal exosome, corresponding to Phe68 in *M. smegmatis* PNPase) over the N4 nucleobase. The kinetic profile of the phosphorolysis reaction of mycobacterial PNPase with the all-RNA strand indicated that PNPase rapidly resected the strand to yield a 5' ^{32}P-labeled trinucleotide (within 10 s), which was then converted slowly (over the course of 5 min) to a mononucleotide end-product. The tetranucleotide substrate complex visualized in the archaeal exosome, with the N4 base clamped in the active site by the overlying enzymic π stack, reflects the state of affairs prior to the phosphorolysis step that generates the kinetically paused trinucleotide end product. We envision that the ejection of the NDP product and movement of the new trinucleotide 3' end into the P1 site, with accompanying loss of the π clamp, destabilizes the interaction of the trinucleotide with PNPase, such that the last two cycles of phosphorolysis to yield a mononucleotide are slower (and non-processive). This structure-based interpretation also rationalizes earlier biochemical studies[21] of the effects of oligoadenylate $(pA)_n$ chain length on the K_m of *M. luteus* PNPase for phosphorolysis, whereby: (1) four or five nucleotides sufficed for relatively high-affinity binding; and (2) the transition from $(pA)_4$ to $(pA)_3$ elicited a 20-fold increase in K_m.

The tetranucleotide-bound exosome structure also provides a frame of reference for the durably arrested state of PNPase with a 3' ribonucleotide in the P1 site and three deoxynucleotides at P2, P3 and P4. Within the tetranucleotide segment, there are several ribose-specific interactions in addition to the hydrogen bond of the terminal ribose O2' with the main-chain carbonyl mentioned above. These are: (i) a van der Waals contact of the N3 nucleoside ribose O2’ with a conserved arginine (corresponding to Arg112 in *M. smegmatis* PNPase); and (ii) a bifurcated contact of the N4 nucleoside ribose O2' with a main-chain carbonyl and the same conserved arginine (Arg112). The ribose-specific interactions of N4 appear not to be crucial for avoidance of DNA-induced pausing, insofar as processing of the $pR_{10}D_2R_{12OH}$ strand was hung up with deoxynucleotides at N2 and N3 and a ribonucleotide at N4. Yet, the sharp transition from a relatively durable pause to transient pause that occurred when the N2 position was a deoxynucleotide and N3 was a ribonucleotide suggests that an N3 deoxyribose sugar does contribute to the longevity of the arrested state.

The salient finding was that even a single deoxynucleotide in the N2 position elicited a transient kinetic delay in phosphorolysis by mycobacterial PNPase. How might this be explained, given that there are no protein contacts to the N2 ribose O2' seen in the archaeal exosome structure? We suggest that the catalytic metal ion is the decisive influence in the DNA-induced impediment to phosphorolysis. The active site of the RNA-bound archaeal exosome lacks a catalytic metal because the enzyme was intentionally mutated so that the one of two conserved metal-binding aspartates was replaced by alanine.[19] The position of the missing aspartate, corresponding to Asp526 in *M. smegmatis* PNPase, is denoted in Fig. 8 by the asterisk overlying its Cα atom. By superimposing the *E. coli* PNPase•Mn^{2+} complex (pdb 3GME) on the archeal exosome•RNA complex, we can surmise the position and role of the catalytic metal, as follows. We propose that the metal ion coordinates (in

addition to the two enzymic aspartates) the non-bridging oxygen (OP1) and the bridging O3' oxygen of the scissile phosphodiester. The former contact aids in stabilization of the presumptive pentacoordinate phosphorane transition state, while the latter contact promotes expulsion of the O3' leaving group. We suggest that the ribose O2' atom of the penultimate (N2) nucleoside is also a component of the metal coordination complex, either as a direct metal ligand or via a bridging water. This model rationalizes the observed effects of an N2 deoxynucleoside, insofar as elimination of the 2'-OH would perturb the Mg^{2+} coordination complex in the PNPase active site, with attendant slowing of the rate of phosphorolysis. Given that PNPase has a modest capacity to resect DNA when Mn^{2+} is the metal cofactor, we surmise that Mn^{2+} is better able than Mg^{2+} to promote PNPase catalysis when the N2 ribose O2' is unavailable to participate in metal coordination.

Acknowledgments

This research was supported by NIH grant AI64693. S.S. is an American Cancer Society Research Professor.

REFERENCES

1. Littauer UZ, Soreq H. Polynucleotide phosphorylase. The Enzymes. 1982; 15:517–553.
2. Mohanty BK, Kushner SR. Polynucleotide phosphorylase functions both as a 3'-to-5' exonuclease and a poly(A) polymerase in *Escherichia coli*. Proc. Natl. Acad. Sci. USA. 2000; 97:11966–11971. [PubMed: 11035800]
3. Cardenas PP, Carrasco B, Sanchez H, Deikus G, Bechhofer DH, Alonso JC. *Bacillus subtilis* polynucleotide phosphorylase 3'-to-5' DNase activity is involved in DNA repair. Nucleic Acids Res. 2009; 37:4157–4169. [PubMed: 19433509]
4. Cardenas PP, Carzaniga T, Zangrossi S, Briani F, Garcia-Tirado E, Deho G, Alonso JC. Polynucleotide phosphorylase exonuclease and polymerase activities on single-stranded DNA ends are modulated by RecN, SsbA and RecA proteins. Nucleic Acids Res. 2011; 39:9250–9261. [PubMed: 21859751]
5. Gong C, Bongiorno P, Martins A, Stephanou NC, Zhu H, Shuman S, Glickman MS. Mechanism of non-homologous end joining in mycobacteria: a low-fidelity repair system driven by Ku, ligase D and ligase C. Nature Struct. Mol. Biol. 2005; 12:304–312. [PubMed: 15778718]
6. Aniukwu J, Glickman MS, Shuman S. The pathways and outcomes of mycobacterial NHEJ depend on the structure of the broken DNA ends. Genes & Development. 2008; 22:512–527. [PubMed: 18281464]
7. Sinha KM, Unciuleac MC, Glickman MS, Shuman S. AdnAB: a new DSB-resecting motor-nuclease from Mycobacteria. Genes & Development. 2009; 23:1423–1437. [PubMed: 19470566]
8. Gupta R, Barkan D, Redelman-Sidi G, Shuman S, Glickman MS. Mycobacteria exploit three genetically distinct DNA double-strand break repair pathways. Mol. Microbiol. 2011; 79:316–330. [PubMed: 21219454]
9. Gupta R, Ryzhikov M, Koroloeva O, Unciuleac M, Shuman S, Korolev S, Glickman M. A dual role for mycobacterial RecO in RecA-dependent homologous recombination and RecA-independent single-strand annealing. Nucleic Acids Res. 2013; 41:2284–2295. [PubMed: 23295671]
10. Unciuleac M, Shuman S. Distinctive effects of domain deletions on the manganese-dependent DNA polymerase and DNA phosphorylase activities of *Mycobacterium smegmatis* polynucleotide phosphorylase. Biochemistry. 2013; 52:2967–2981. [PubMed: 23560592]
11. Symmons MF, Jones GH, Luisi BF. A duplicated fold is the structural basis for polynucleotide phosphorylase catalytic activity, processivity, and regulation. Structure. 2000; 8:1215–1226. [PubMed: 11080643]
12. Shi Z, Yang WZ, Lin-Chao S, Chak KF, Yuan HS. Crystal structure of *Escherichia coli* PNPase: central channel residues are involved in processive RNA degradation. RNA. 2008; 14:2361–2371. [PubMed: 18812438]
13. Nurmohamed S, Vaidialingam B, Callaghan AJ, Luisi BF. Crystal structure of *Escherichia coli* polynucleotide phosphorylase core bound to RNase E, RNA and manganese: implications for

catalytic mechanism and RNA degradosome assembly. J. Mol. Biol. 2009; 389:17–33. [PubMed: 19327365]

14. Lin CH, Wang yT, Yang WZ, Hsiao YY, Yuan HS. Crystal structure of human polynucleotide phosphorylase: insights into its domain function in RNA binding and degradation. Nucleic Acids Res. 2012; 40:4146–4157. [PubMed: 22210891]
15. Hardwick SW, Gubbey T, Hug I, Jenal U, Luisi BF. Crystal structure of *Caulobacter crescentus* polynucleotide phosphorylase reveals a mechanism of RNA substrate channeling and RNA degradosome assembly. Open Biol. 2012; 2:120028. [PubMed: 22724061]
16. Das U, Shuman S. Mechanism of RNA 2',3'-cyclic phosphate end-healing by T4 polynucleotide kinase-phosphatase. Nucleic Acids Res. 2013; 41:355–365. [PubMed: 23118482]
17. Jarrige AC, Brechemier-Baey D, Mathy N, Duche O, Portier C. Mutational analysis of polynucleotide phosphorylase from *Escherichia coli*. J. Mol. Biol. 2002; 321:397–409. [PubMed: 12162954]
18. Lorentzen E, Dziembowski A, Lindner D, Seraphin B, Conti E. RNA channeling by the archaeal exosome. EMBO reports. 2007; 8:470–476. [PubMed: 17380186]
19. Lorentzen E, Conti E. Crystal structure of a 9-subunit archaeal exosome in pre-catalytic states of the phosphorolytic reaction. Archaea. 2012; 2012:721869. [PubMed: 23319881]
20. Chou JY, Singer MF. A kinetic analysis of the phosphorolysis of oligonucleotides by polynucleotide phosphorylase. J. Biol. Chem. 1970; 245:995–1004. [PubMed: 4313707]
21. Chou JY, Singer MF. The effect of chain length on the phosphorolysis of oligonucleotides by polynucleotide phosphorylase. J. Biol. Chem. 1970; 245:1005–1011. [PubMed: 4313699]
22. Zhu H, Shuman S. Novel 3'-ribonuclease and 3'-phosphatase activities of the bacterial non-homologous end-joining protein, DNA ligase D. J. Biol. Chem. 2005; 280:25973–25981. [PubMed: 15897197]
23. Nair PA, Smith P, Shuman S. Structure of bacterial LigD 3'-phosphoesterase unveils a DNA repair superfamily. Proc. Natl. Acad. Sci. USA. 2010; 107:12822–12827. [PubMed: 20616014]

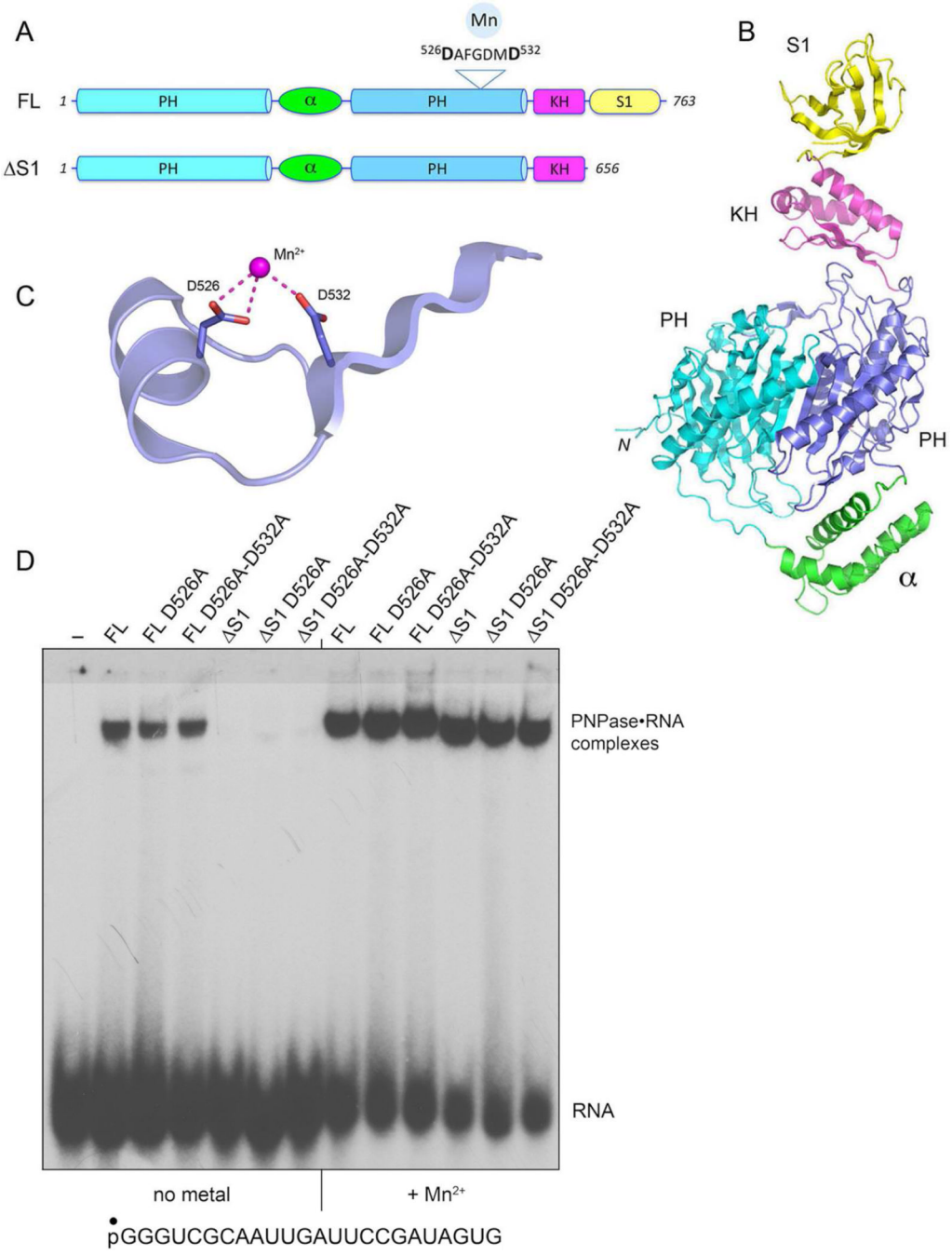

Figure 1. Domain organization of mycobacterial PNPase and effects of metal ligand mutations on nucleic acid binding

(A) The modular domain structures of full-length (FL) *M. smegmatis* PNPase and the ΔS1 variant are shown. The sequence motif comprising the metal-binding site in the distal PH domain is highlighted. (B) The tertiary structure of the homologous FL PNPase of *Caulobacter crescentus* (pdb ID 4AIM) is shown. (C) The Mn^{2+}-binding site in the *E. coli* PNPase•Mn^{2+} crystal structure (pdb ID 3GME) is shown; the aspartates are numbered according to their position in *M. smegmatis* PNPase. (D) Electrophoretic mobility shift assay of RNA binding by FL and ΔS1 PNPase was performed as described under Methods. The free ^{32}P-labeled 24-mer RNA (sequence shown at bottom) and slower migrating

PNPase•[^{32}P]-nucleic acid complexes were resolved by native PAGE and visualized by autoradiography.

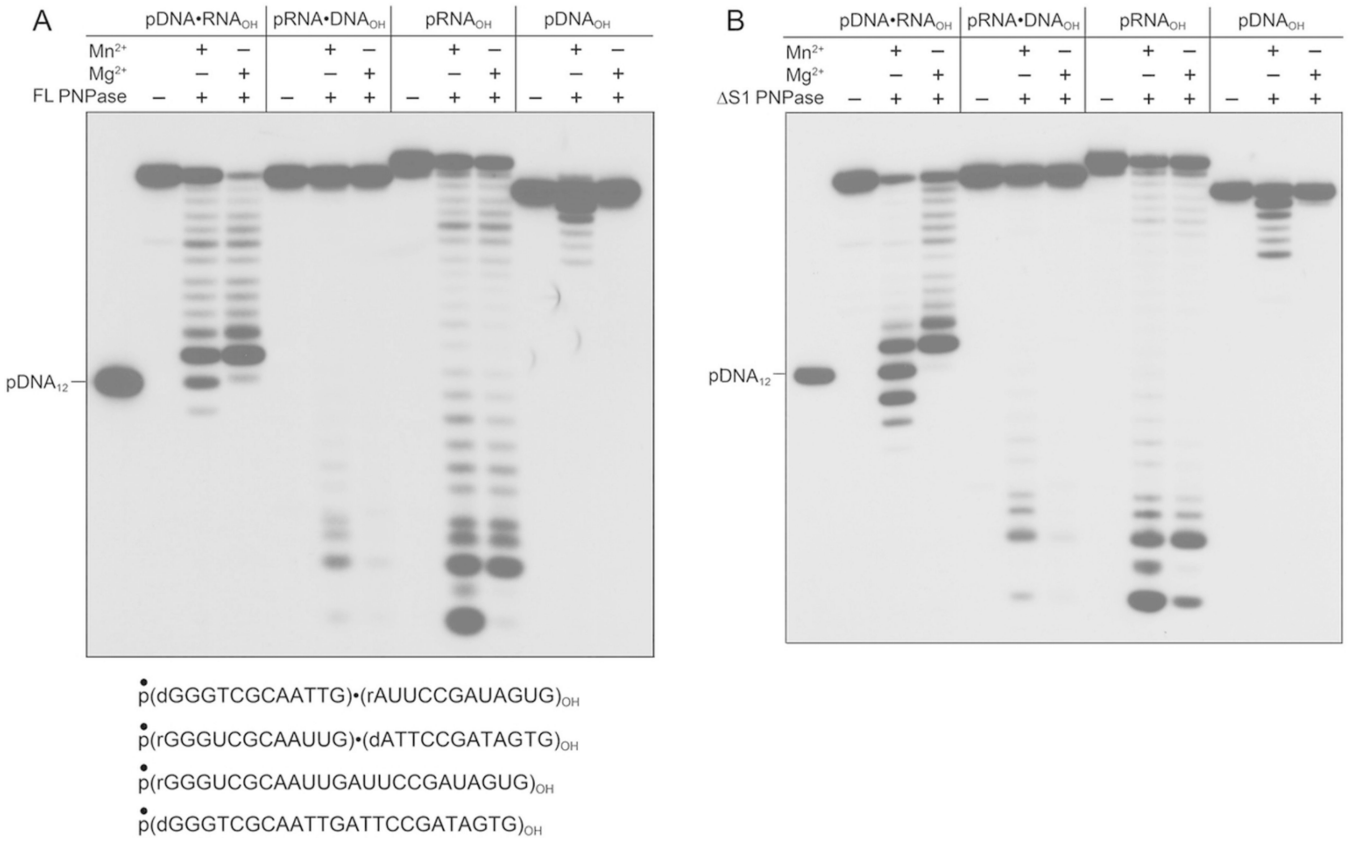

Figure 2. DNA imposes a kinetic obstacle to 3' phosphorolysis

Reaction mixtures (10 μl) containing 20 mM Tris-HCl (pH 7.5), 5 mM $MnCl_2$ or 5 mM $MgCl_2$ (where indicated by +), 30 μM $(NH_4)_2PO_4$, 0.1 μM 5' ^{32}P-labeled 24-mer polynucleotide substrate as specified (either $pDNA_{OH}$, $pRNA_{OH}$, or $pDNA•RNA_{OH}$ or $pRNA•DNA_{OH}$ chimeras, shown at the bottom with the radiolabel denoted by ●), and either 0.1 μM full-length PNPase protomer (panel A) or 0.3 μM ΔS1 PNPase protomer (panel B) were incubated for 15 min at 37°C. The products were resolved by urea-PAGE and visualized by autoradiography. A 5' ^{32}P-labeled 12-mer DNA strand $pGGGTCGCAATTG_{OH}$ ($pDNA_{12}$) corresponding to the DNA segment of the pDNA•RNA chimera was analyzed in parallel in the left lanes of the gels.

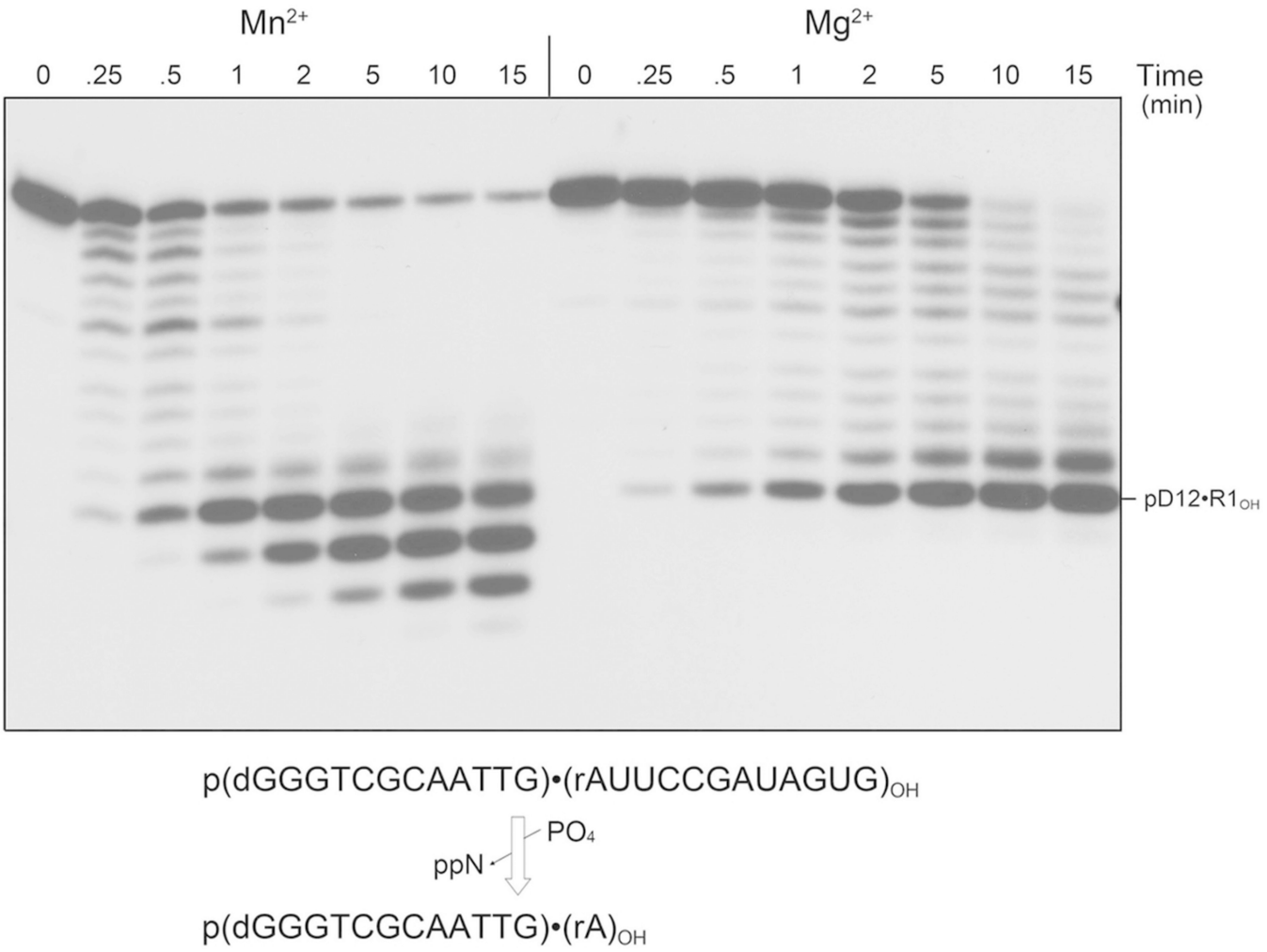

Figure 3. Time course of pDNA•RNA$_{OH}$ phosphorolysis

Reaction mixtures (80 μl) containing 20 mM Tris-HCl (pH 7.5), 5 mM $MnCl_2$ or 5 mM $MgCl_2$ as specified, 30 μM $(NH_4)_2PO_4$, 0.1 μM 5' ^{32}P-labeled pDNA•RNA$_{OH}$ substrate and 0.3 μM ΔS1 PNPase protomer were incubated at 37°C. Aliquots (10 μl) were withdrawn at the times specified and quenched with formamide/EDTA. The reaction products were analyzed by urea-PAGE and visualized by autoradiography.

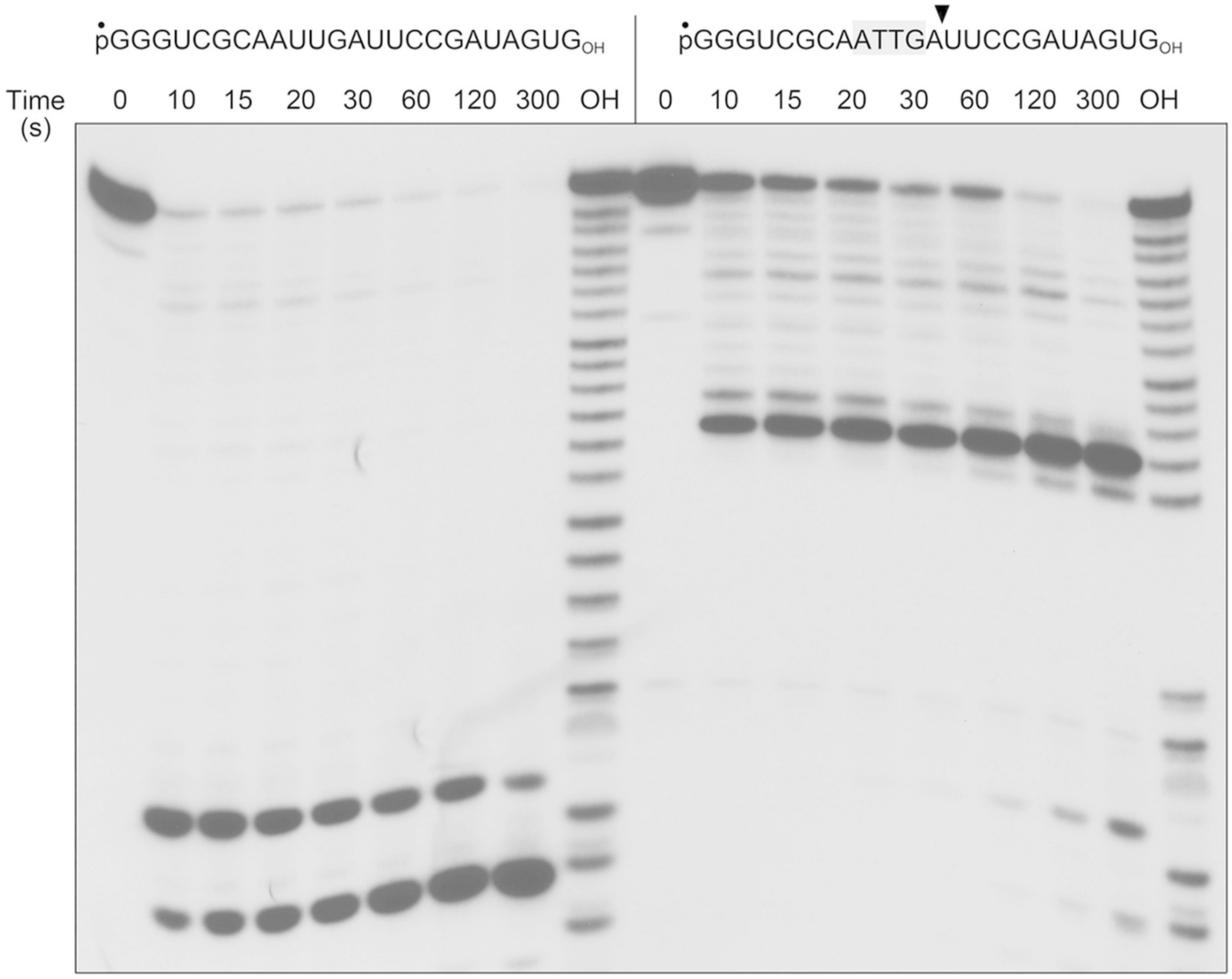

Figure 4. A tract of four internal deoxynucleotides suffices to arrest phosphorolysis

Reaction mixtures (80 μl) containing 20 mM Tris-HCl (pH 7.5), 5 mM $MgCl_2$, 0.5 mM $(NH_4)_2PO_4$, 0.3 μM FL PNPase protomer, and 0.1 μM 5' ^{32}P-labeled 24-mer polynucleotide as specified, either an all-RNA strand (left panel) or an RNA with four consecutive internal deoxyribonucleotides (right panel, with deoxys highlighted in gray) were incubated at 37°C. Aliquots (10 μl) were withdrawn at the times specified and quenched with formamide/EDTA. The reaction products were analyzed by urea-PAGE and visualized by autoradiography. The samples in lanes OH are partial alkaline hydrolysates of the respective 5' ^{32}P-labeled 24-mer polynucleotides, prepared by incubation in a solution of 40 mM $NaHCO_3$, 60 mM Na_2CO_3 (pH 10.2) for 12 min at 95°C.

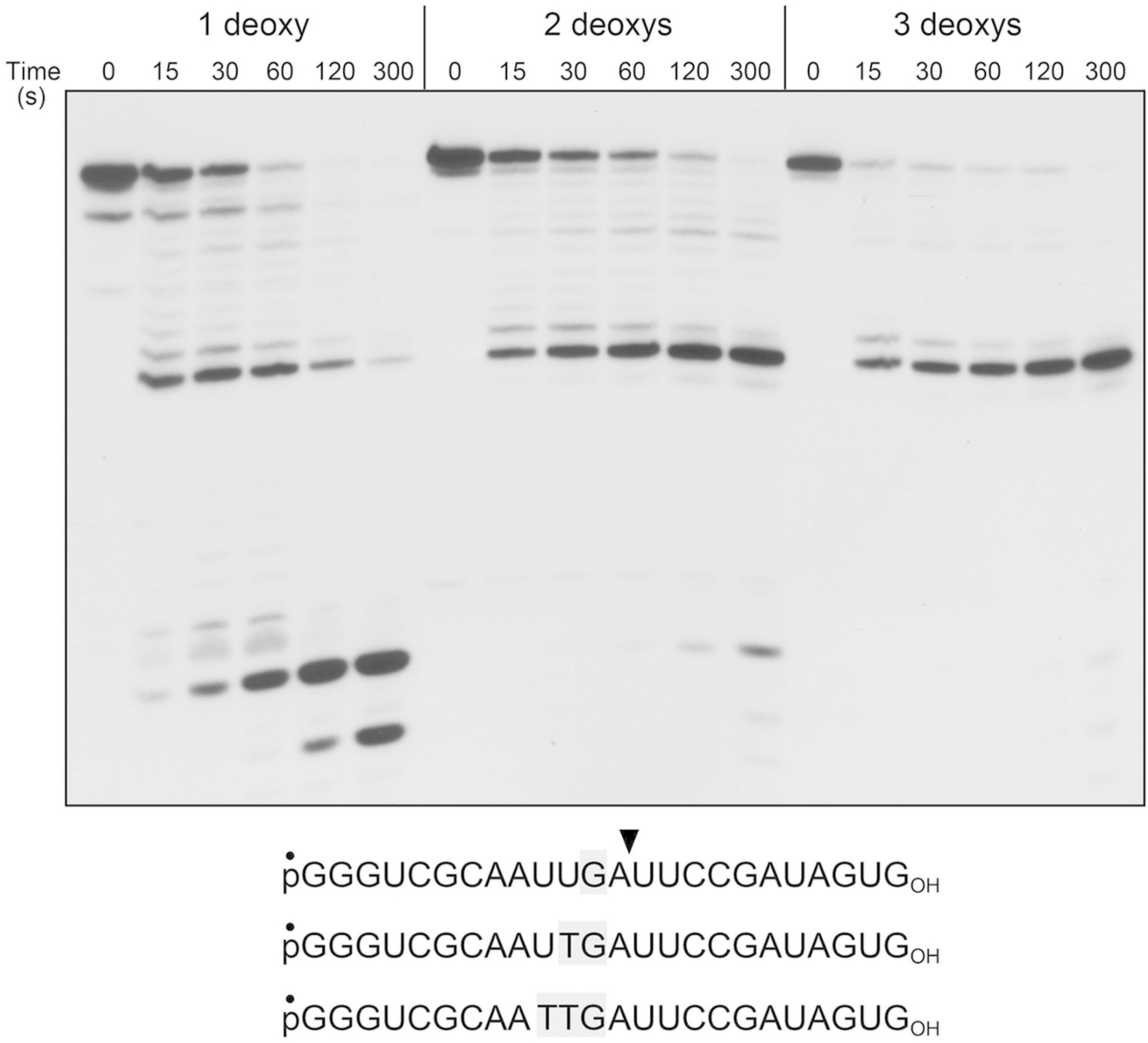

Figure 5. Effect of three, two and one internal deoxynucleotides

Reaction mixtures (80 μl) containing 20 mM Tris-HCl (pH 7.5), 5 mM $MgCl_2$, 0.5 mM $(NH_4)_2PO_4$, 0.3 μM FL PNPase protomer, and 0.1 μM 5' ^{32}P-labeled 24-mer RNA with three, two or one internal deoxyribonucleotides (shown at bottom, with deoxys highlighted in gray) were incubated at 37°C. Aliquots (10 μl) were withdrawn at the times specified and quenched with formamide/EDTA. The reaction products were analyzed by urea-PAGE and visualized by autoradiography.

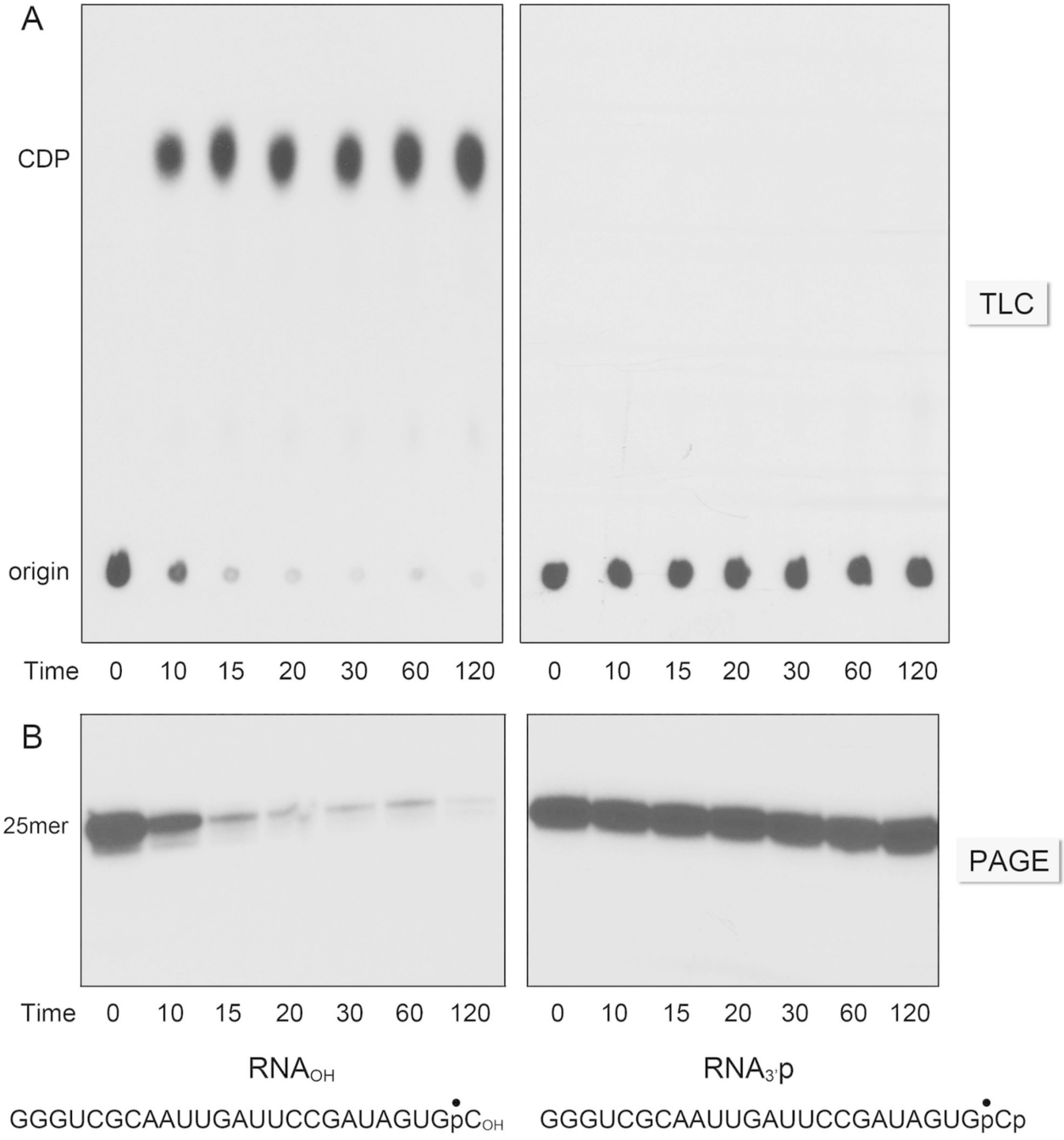

Figure 6. Can PNPase process "dirty" 3'-PO$_4$ ends?

Phosphorolysis of 3' ^{32}P-labeled 25-mer RNAp or RNA$_{OH}$ substrates (shown at bottom) by full-length PNPase in the presence of magnesium was assayed as described in Experimental Procedures. The reactions were quenched at the times specified and the products were analyzed in parallel by PEI-cellulose TLC (panel A) and urea-PAGE (panel B).

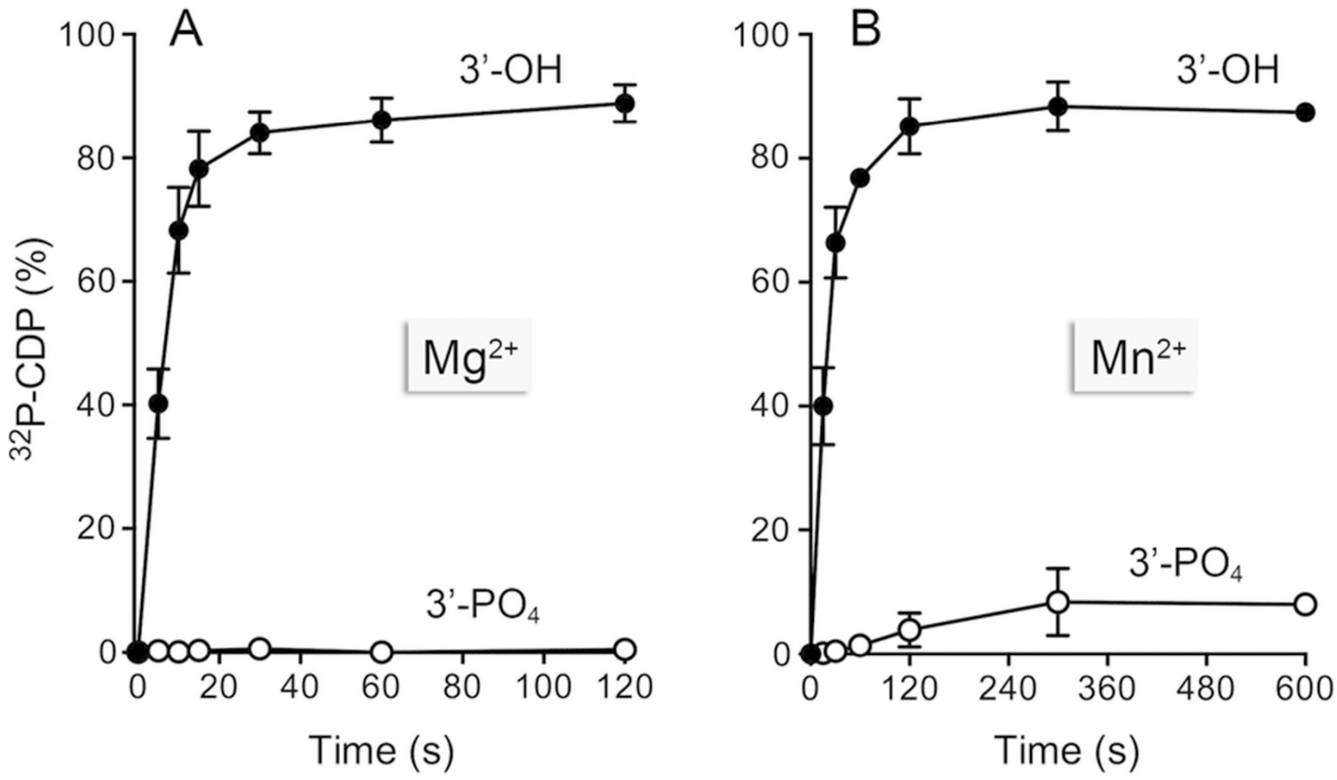

Figure 7. Kinetics of processing of 3'-OH versus 3'-PO_4 substrates

Phosphorolysis of 3' ^{32}P-labeled 25-mer RNAp or RNA_{OH} substrates by full-length PNPase in the presence of magnesium (panel A) or manganese (panel B) was assayed as described in Experimental Procedures. The reactions were quenched at the times specified and the products were analyzed by PEI-cellulose TLC. The extent of ^{32}P-CDP release (as % of total radioactivity) is plotted as a function of reaction time. Each datum in the graphs is the average of three separate experiments ±SEM.

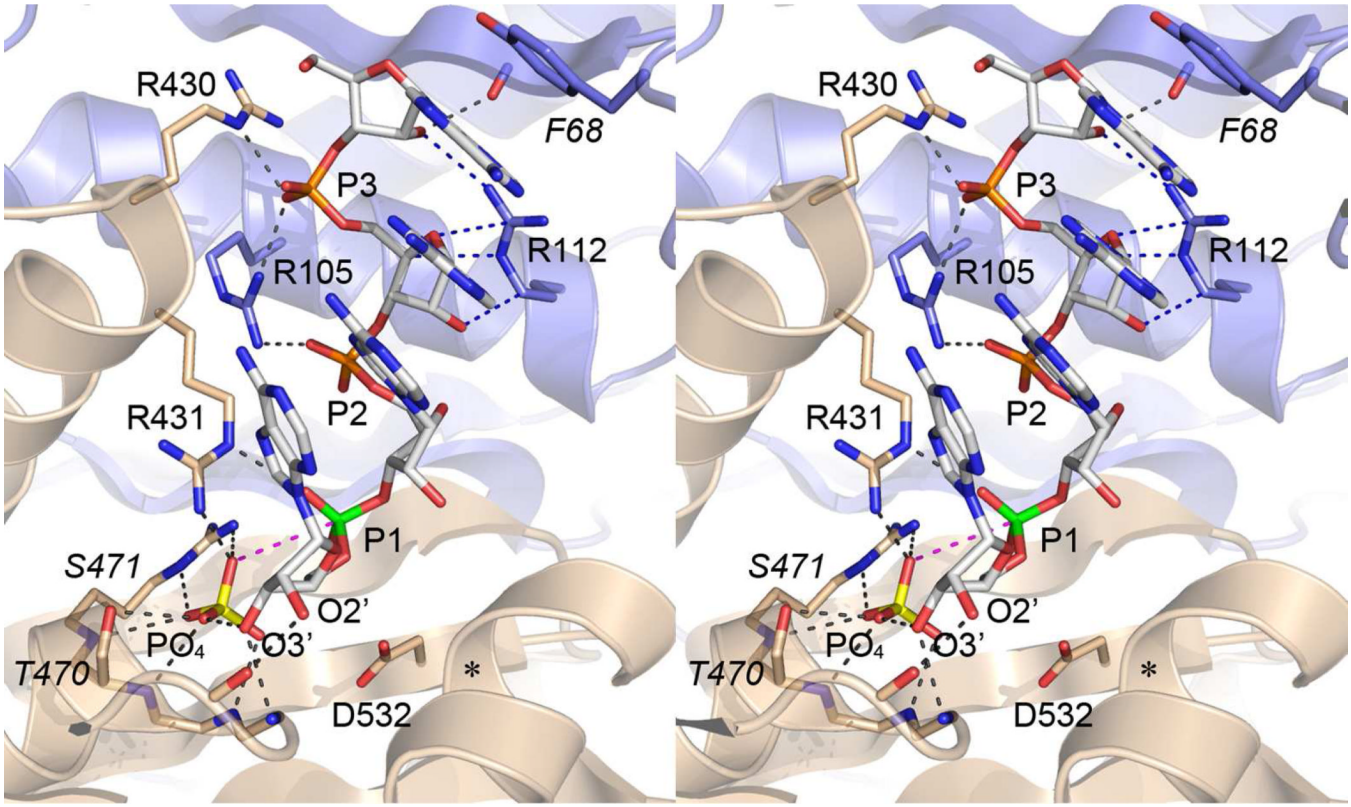

Figure 8. Insights to PNPase catalysis from the archaeal exosome structure

Stereo view of the active site of the archaeal exosome (from pdb ID 4BA2) with an RNA_{OH} and inorganic phosphate bound. The polypeptides corresponding to the proximal and distal PH domains in PNPase are colored blue and beige, respectively. The phosphorus atom of the 3'-terminal phosphodiester is colored green. The path of nucleophilic attack of the phosphate anion (depicted with a yellow phosphorus atom) on the scissile phosphodiester (P1) is denoted by the magenta dashed line. Hydrogen bonding and electrostatic contacts to the RNA and inorganic phosphate ligands are denoted by dashed black lines. The side chains are labeled and numbered according to their counterparts in mycobacterial PNPase. Identical side chains are labeled in regular font. Non-identical side chains are labeled in italics.